# SYSTEMATIC ANALYSES OF RADIOCARBON AGES OF COEXISTING PLANKTONIC FORAMINIFERA

Jörg Lippold[1]*  • Julia Gottschalk[2]  • Jean Lynch-Stieglitz[3]  •
Matthew W Schmidt[4]  • Sönke Szidat[5]  • Andre Bahr[1]

[1]Institute of Earth Sciences, Heidelberg University, Heidelberg, Germany
[2]Institute of Geosciences, Kiel University, Kiel, Germany
[3]School of Earth and Atmospheric Sciences, Georgia Institute of Technology, Atlanta, GA, USA
[4]Department of Ocean and Earth Sciences, Old Dominion University, Norfolk, VA, USA
[5]University of Bern, Department of Chemistry, Biochemistry and Pharmaceutical Sciences & Oeschger Centre for Climate Change Research, Bern, Switzerland

**ABSTRACT.** We compare radiocarbon ($^{14}$C) ages of coexisting planktonic foraminifera species from sediment cores VM12-107 and KNR166-2-26JPC from the Equatorial Atlantic Ocean for three time periods (Holocene, Heinrich Stadial 1, last glacial maximum). We find a maximum inter-species difference of 1200 $^{14}$C yr. On average, the $^{14}$C ages deviate by ∼300 yr between *Globigerinoides ruber* and other species. In most cases, this exceeds the analytical uncertainty range of the measurements and thus renders the choice of species for generating age models as important as sample weight. While modern stratified water-column profiles imply an increase in $^{14}$C ages with water depth, we observe an expected parallel increase of $^{14}$C ages and $\delta^{18}$O only at VM12-107. The mismatch between $^{14}$C ages and $\delta^{18}$O at KNR166-2-26JPC likely results from the effects of bioturbation and the hydrographic setting. The largest difference in $^{14}$C ages between mixed-layer versus thermocline-calcifying planktonic foraminifera are observed during Heinrich Stadial 1 despite a decrease in upper-ocean stratification at that time. This difference is likely the result of inconsistent increases in $^{14}$C reservoir ages during times of reduced overturning circulation masking the potential of $^{14}$C ages of coexisting planktonic foraminifera to reflect the density stratification of the water column.

KEYWORDS: $^{14}$C ages, coexisting planktic foraminifera, Heinrich Stadial, Holocene, Last Glacial Maximum.

## INTRODUCTION

For the time range younger than ∼50 ka BP, radiocarbon ($^{14}$C) ages derived from planktonic foraminifera tests represent the most important toolbox for absolute dating of marine sediment cores (e.g. Skinner and Bard 2022). Known uncertainties and limitations of this method include bioturbation, atmospheric $^{14}$C changes, selective test dissolution or poorly constrained reservoir ages (Löwemark and Schäfer 2003; Ascough et al. 2009; Mekik 2014; Stern and Lisiecki 2014; Ezat et al. 2017; Küssner et al. 2018). It is often unclear to what extent these processes account for the significant differences observed in the $^{14}$C ages of coexisting planktonic foraminifera (Andree et al. 1984; Broecker et al. 1984; Peng and Broecker 1984; Bard et al. 1987; Manighetti and McCave 1995; Löwemark and Grootes 2004; Broecker et al. 2006; Barker et al. 2007; Lindsay et al. 2015; Mekik 2014; Wycech et al. 2016; Ausin et al. 2019). Such offsets imply that $^{14}$C ages of planktonic foraminifera derived from marine sediment cores might not always faithfully reflect the depositional age of the surrounding sediment material (Mollenhauer et al. 2005; Ausin et al. 2019). Considering the fundamental role of a robust age model for any paleoceanographic interpretation, it is important to better understand the significance and drivers of planktonic foraminiferal inter-species $^{14}$C age offsets. However, so far, only few studies have addressed this topic in a systematic way—possibly a consequence of the high cost of high-quality accelerator mass spectrometry (AMS) analyses, scarce foraminiferal abundances in sediments (putting severe restrictions on the AMS measurements technique) and the difficulty to parse out various processes driving inter-species $^{14}$C age offsets.

---

*Corresponding author. Email: joerg.lippold@geow.uni-heidelberg.de

The $^{14}$C age difference between co-occurring benthic (bottom-calcifying) and planktonic (surface-calcifying) foraminifera is a well-established proxy for deep ocean ventilation, which builds on the realization that they faithfully reflect the $^{14}$C signature of the water mass they grew in (Rafter et al. 2022). This proxy follows the rationale that deep-water masses acquire an older $^{14}$C signature than the surface ocean, which is in constant exchange with the atmosphere (Peng and Broecker 1984; Thornalley et al. 2011; Cook and Keigwin 2015). All else constant, a similar difference in $^{14}$C signature can be expected from coexisting surface- and thermocline-calcifying foraminifera as the natural $^{14}$C content ($\Delta^{14}$C) of dissolved inorganic carbon (DIC) decreases markedly below the seasonal thermocline given the influence of $^{14}$C-depleted sub-surface waters. Thus, in stratified ocean areas, distal to regions of upwelling or subsurface water formation, foraminifera calcifying in the deep thermocline such as *Globorotalia crassaformis* and *Globorotalia truncatulinoides* should accordingly show older $^{14}$C ages than shallower, mixed-layer species such as *Globigerinoides ruber* and *Trilobatus sacculifer* (Fairbanks et al. 1980; Fairbanks et al. 1982; Schmuker and Schiebel 2002; Cleroux et al. 2007; Regenberg et al. 2009; Cleroux and Lynch-Stieglitz 2010; Schiebel and Hemleben 2017).

Here we aim to estimate the depth gradients in $^{14}$C among five coexisting planktonic foraminifera species that calcify in different water depths between mixed layer and deep thermocline for three time slices in the past. We further investigate the extent to which these potential gradients can be explained by past water column $^{14}$C gradients. Changes in water column $^{14}$C gradients are expected for times of thermocline shifts. For instance, thermocline deepening in the low latitudes of the Atlantic Ocean is documented by high Mg/Ca paleo-temperatures reconstructed from thermocline-calcifying foraminifera during high-latitude cold events in the past, such as Heinrich Stadial 1 (HS1), and to a weaker extent during the last glacial maximum (LGM; Chiessi et al. 2008; Lopes dos Santos et al. 2010; Bahr et al. 2011; Schmidt et al. 2012; Bahr et al. 2013a; Nürnberg et al. 2015; Reißig et al. 2019). We hypothesize that $^{14}$C age offsets between mixed-layer and thermocline-calcifying foraminifera varied with these changes in upper ocean configuration, with a weaker stratification leading to a smaller $^{14}$C age offset between coexisting planktonic foraminifera. Our analyses also help to estimate age uncertainties potentially introduced by the choice of planktonic foraminiferal species selected for $^{14}$C age dating.

For this study, we have chosen two well-studied high-sedimentation study sites: sediment core KNR166-2-26JPC from Florida Straits and VM12-107 from the Caribbean Sea. In order to examine past geochemical variations of the water column at our study sites, we investigated $^{14}$C ages and $\delta^{18}$O of coexisting planktonic foraminifera during time slices that are characteristic for different states of ocean hydrography at both sites: the LGM, representative of a glacial background state (~19–24 ka before present, BP), HS1 characterized by strong heat accumulation and weak upper ocean stratification in the low latitudes (~15–17 ka BP, references for weaker upper ocean stratification), and the late Holocene as a reference for present-day interglacial conditions (samples from ~1 ka BP).

## STUDY AREA, METHODS, AND MATERIAL

### Selection of Study Sites

We studied sediment cores VM12-107 (11°19.8'N, 66°37.8'W; 1,079 m) from Bonaire Basin in the Eastern Caribbean Sea (Schmidt et al. 2012) and KNR166-2-26JPC (24°19.6'N, 83° 15.1'W; 546 m) from the Florida Straits (Schmidt and Lynch-Stieglitz 2011; Lynch-Stieglitz et al. 2014; Figure 1). Both sites host a high number of foraminifera tests that are characterized
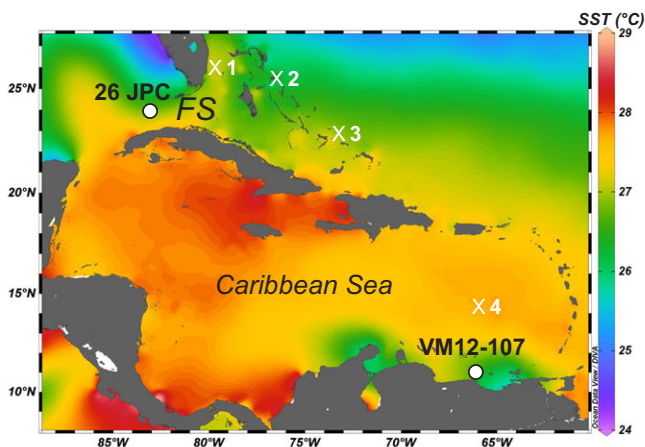
Figure 1   Location of our study cores superimposed on map of annual mean sea surface temperatures (SST; Boyer et al. 2013) in the Caribbean Sea and Florida Straits (FS) regions. Circles denote locations of our study cores KNR166-2-26JPC (abbreviated with 26JPC) and VM12-107. Crosses indicate the water column stations from Global Ocean Data Analysis Project (Olsen et al. 2019): X1 = 29HE19920714#107, X2 = 316N19810401#15, X3 = 316N19810401#16, X4 = 316N19821201#4. Map was created using Ocean Data View (Schlitzer 2016).

by a high level of preservation and that are sufficient for the sample demands of ^{14}C dating with an AMS equipped with gas ion source such as the mini-carbon dating system (MICADAS). Further, both have a moderate-to-high diversity of shallow and deep-calcifying planktonic foraminifera species, exhibit high sedimentation rates around or in excess of 10 cm/kyr and are sensitive to oceanographic changes (in particular upper-ocean stratification) during the late Pleistocene (Schmidt et al. 2012; Lynch-Stieglitz et al. 2014).

The chronostratigraphies of both cores are constrained by AMS ^{14}C dating of mixed *Trilobatus sacculifer/Trilobatus trilobus* and *G. ruber* specimens (Figure 2), and additionally by the correlation of planktonic foraminiferal $\delta^{18}O$ and Mg/Ca-based SST with the Greenland $\delta^{18}O$ ice-core and the Hulu speleothem record (Lynch-Stieglitz et al. 2011; Schmidt and Lynch-Stieglitz 2011; Lynch-Stieglitz et al. 2014; Schmidt et al. 2012). Average sedimentation rates for the three selected intervals are high (16–23 cm/kyr in core KNR166-2-26JPC and 9-16 cm/kyr in core VM12-107; Figure 2), hence minimizing the potential effect of bioturbation on the ^{14}C ages of different planktonic foraminifera (Barker et al. 2007; Wycech et al. 2016).

Both locations exhibited distinct changes in the upper-ocean structure during the past ~20 kyr (Lynch-Stieglitz et al. 2014; Schmidt et al. 2012). This is in particular true for periods of weaker Atlantic meridional overturning circulation (AMOC) such as during HS1 and the Younger Dryas (YD) cold period, as inferred from [231]Pa/[230]Th records (Ng et al. 2018). In the case of Caribbean Site VM12-107, both intervals are characterized by subsurface warming and decreased upper-water column density stratification due to the influence of salty, warm subtropical gyre waters that flow southward during periods of reduced AMOC (Schmidt et al. 2012). Similarly, planktonic foraminiferal stable oxygen isotopes from core KNR166-2-26JPC suggest a decrease of the northward water mass transport through Florida Straits, which is thought to have considerably reduced upper-ocean density stratification during HS1 and the YD (Lynch-Stieglitz et al. 2014).
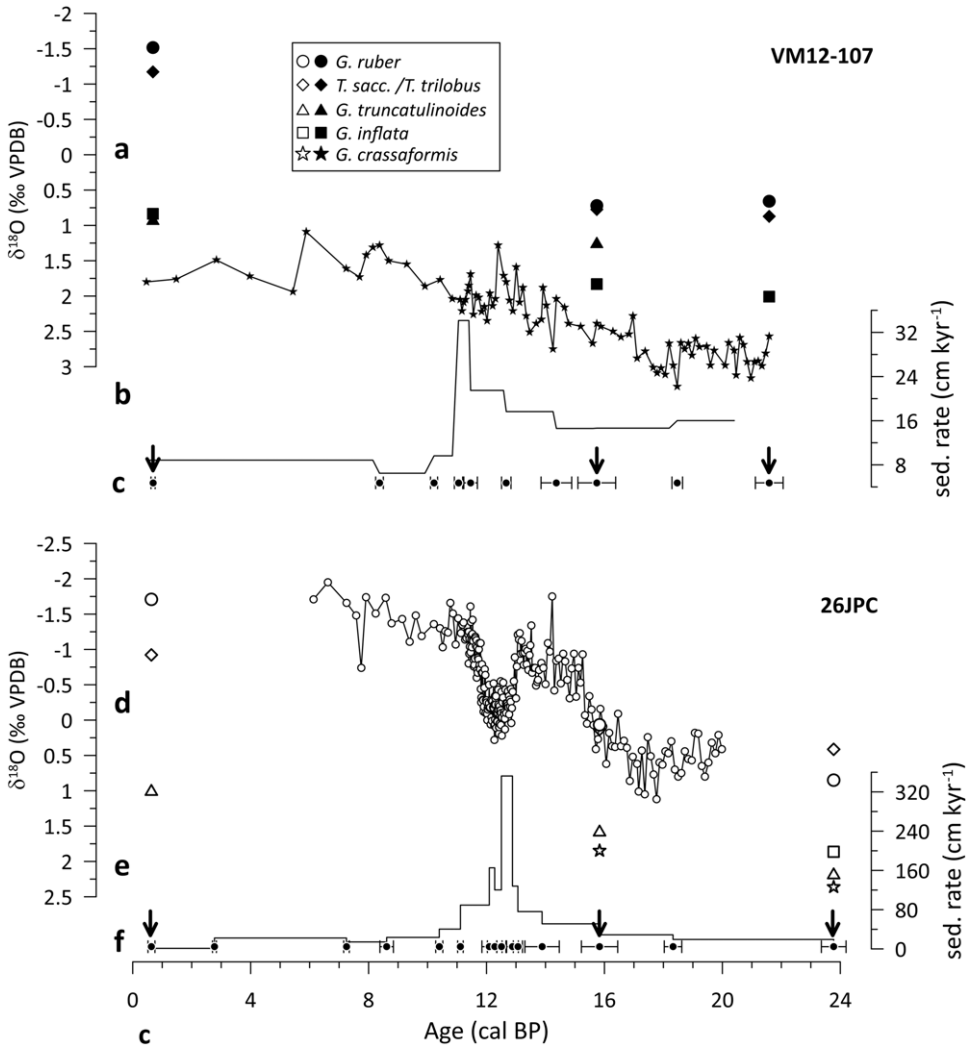
Figure 2   Time-series overview at our two study sites, VM12-107 (top) and KNR166-2-26JPC, referred to as 26JPC (bottom). a, d) Planktonic foraminiferal δ¹⁸O records; b, e) sedimentation rates and c, f) age control points (Lynch-Stieglitz et al. 2011, 2014; Schmidt and Lynch-Stieglitz 2011; Schmidt et al. 2012; this study). Black arrows indicate examined time-slices.

In the tropical and sub-tropical regions of the Atlantic Ocean, different habitat- and by inference calcification depths of planktonic foraminifera span a gradient of ~60‰ in natural (i.e., bomb-corrected) $\Delta^{14}C$ concentrations in the top 1000 m of the water column (Figure 3). Pre-bomb seawater $^{14}C$ concentrations ($\Delta^{14}C$) in our study area are high in the upper 200 m of the water column (Olsen et al. 2019), while they decline due to the admixture of "old" $^{14}C$ from underlying intermediate water masses (here Antarctic Intermediate Water) below 200 m (Figure 3). We hence argue that given the pre-bomb water column $\Delta^{14}C$ profile at our study sites the $\Delta^{14}C$ difference between the deepest-calcifying foraminifera *G. crassaformis* and shallowest-calcifying foraminifer *G. ruber* should be about 30–60‰ translating into a $^{14}C$ age difference of approximately 230–470 $^{14}C$ yr. This is generally higher than the uncertainty range
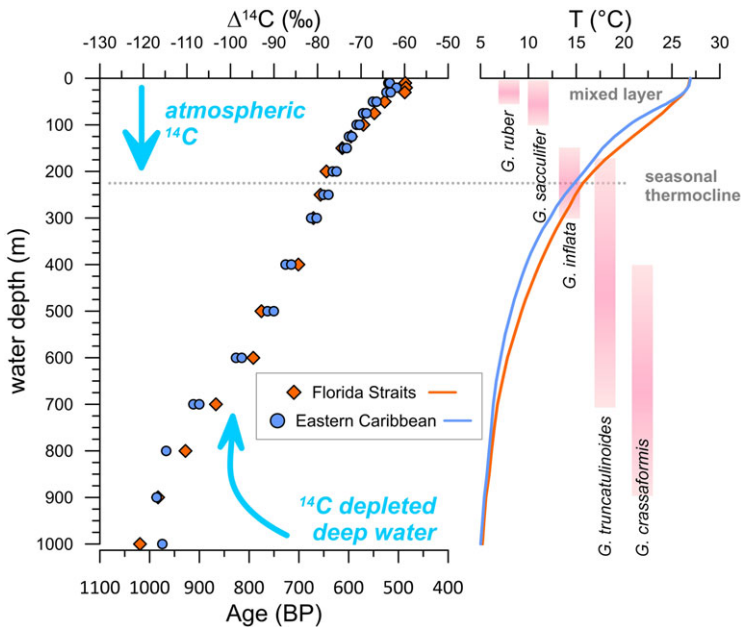
Figure 3   $\Delta^{14}$C signatures in the upper water column of the study area in relation to ocean temperatures and planktonic foraminiferal calcification and habitat depths. Left: Bomb-corrected seawater $^{14}$C concentrations ($\Delta^{14}$C) at Station 316N19821201#4 in the Eastern Caribbean Sea (blue circles) and Stations 29HE19920714#107, 316N19810401#15 and 316N19810401#16 in the Florida Straits (red diamonds) from Global Ocean Data Analysis Project (Olsen et al. 2019). The average relative error range of the $\Delta^{14}$C values is 5 %. Right: Annual mean temperature profiles monitored in proximity to the sediment cores examined in this study (core KNR166-2-26JPC, red line and core VM12-107, blue line, from World Ocean Atlas (Locarnini et al. 2019); see Figure 1 for core locations). Habitat depths (pink bars) approximating calcification depths for the planktonic foraminifera species targeted in this study are inferred either from plankton tow catches (Jentzen et al. 2018b) or core top $\delta^{18}$O estimates from the study area (Cleroux et al. 2007; Regenberg et al. 2009; Steph et al. 2009).

of AMS $^{14}$C dates of last deglacial foraminiferal tests material of around 50–250 yr depending on sample size and $^{14}$C age as obtained for the Bern-MICADAS (Gottschalk et al. 2018). We test if systematic reductions in $^{14}$C age differences between thermocline- and mixed layer-calcifying foraminifera during times of decline in the water-column density stratification can be observed.

**Planktonic foraminifera**

For our study, we selected planktonic foraminiferal species that predominantly calcify in the mixed-layer (*G. ruber* (white and pink), *T. sacculifer*, *T. trilobus*) and the thermocline (*Globorotalia inflata*, *G. truncatulinoides* (d, dextral coiling), *G. crassaformis*), and are sufficiently abundant to carry out $^{14}$C analyses in both cores for all targeted time slices (Figure 3). For *G. ruber* and *T. sacculifer*/*T. trilobus* we analysed the size fraction larger than 250 μm, for *G. inflata*, *G. truncatulinoides* and *G. crassaformis* we used the size fraction larger than 315 μm. In the Caribbean Sea, *G. ruber* (white and pink) is a mixed-layer species dwelling in the upper 30–40 m of the water column, while *T. sacculifer* and *T. trilobus* represent mixed-layer dwellers with an inferred calcification depth that is slightly deeper than that of *G. ruber* (0–100 m) (Schmuker and Schiebel 2002; Regenberg et al. 2009; Steph et al. 2009; Bahr et al. 2013b). In the western subtropical North Atlantic and the Caribbean Sea, *G. inflata* dwells in

the upper thermocline (180–300 m; Cleroux et al. 2007), while *G. truncatulinoides* (d, dextral coiling) is an intermediate to deep thermocline-dweller (170–700 m; Cleroux et al. 2007; Regenberg et al. 2009; Jentzen et al. 2018a). It is believed that encrustation stages of *G. truncatulinoides* reflect different calcification depths (for non-encrusted specimens: 0-150 m, for encrusted: 170-700 m; (Cleroux and Lynch-Stieglitz 2010; Jentzen et al. 2018b; Reynolds et al. 2018). Hence, we only selected well-encrusted specimens to cover a deep thermocline habitat with *G. truncatulinoides* (d). *G. crassaformis* is a deep thermocline-dweller living at the base of the deep thermocline (450–900 m; Regenberg et al. 2009). Using a binocular microscope, we selected only well preserved and intact tests to avoid contamination by reworked and diagenetically altered specimens.

## RADIOCARBON DATING

Low abundances of planktonic foraminifera, often insufficient for conventional AMS $^{14}$C analyses, prohibits systematic in-depth analyses of $^{14}$C age differences between different planktonic foraminiferal species. We took advantage of new advances in AMS techniques via the MICADAS allowing for $^{14}$C analyses of small-sized (foraminiferal) samples (Wacker et al. 2013; Gottschalk et al. 2018; Missiaen et al. 2020). For $^{14}$C analyses (Tables 1 and 2), we used the MICADAS of the University of Bern, Switzerland, fitted with a gas ion source allowing online analysis of small-size samples in gas form following the protocol described by Gottschalk et al. (2018). For larger sample sizes, graphitization has been applied in order to obtain a higher precision of the analyses (Table 2). For four samples with high sample weights (7–10 mg CaCO$_3$), both methods have been applied in order to monitor analytical reproducibility and for direct comparison between graphitization and gas ion source methods. Reported radiocarbon ages are not reservoir age-corrected.

### Stable Oxygen Isotope Analyses

The stable oxygen isotope composition of planktonic foraminifera (here reported in δ-notation with reference to the Vienna Peedee Belemnite (VPDB) standard) has been measured for the three time slices from available foraminiferal species of both cores to constrain the respective states of upper-ocean hydrography. Stable oxygen isotope data were generated from sample depths bracketing the core intervals examined for $^{14}$C (see supplementary table for further details such as sample sizes). Measurement procedures followed the methods previously described by Lynch-Stieglitz et al. (2011). Isotope measurements were performed using a ThermoFisher MAT 253plus mass spectrometer coupled to a Kiel IV device calibrated with the NBS-19 and NBS-18 standards (KNR166-2-26JPC; Georgia Tech) and a ThermoFisher MAT 253plus mass spectrometer coupled to a Kiel IV device calibrated to an in-house Solnhofen limestone standard (VM12-107; Heidelberg University). Analytical precision based on repeated measurements of the in-house standard is lower than 0.06‰ for δ$^{18}$O on both instruments.

### RESULTS

We present 20 new $^{14}$C ages of five planktonic foraminiferal species from sediment core KNR166-2-26JPC and VM12-107, representing the Holocene, HS1 and the LGM (Table 2). These data complement three already available $^{14}$C dates from core KNR166-2-26JPC (Lynch-Stieglitz et al. 2014). Four comparative $^{14}$C measurements with the gas ion source and involving graphitization yielded higher $^{14}$C age uncertainties (average: 160 $^{14}$C yr) for the gas

Table 1    Sample overview. Sample intervals and weights of $^{14}$C-dated planktonic foraminifera species. Some species were absent or not of sufficient abundance to be considered for a reliable AMS measurement.

| Time period | KNR166-2-26JPC | | | VM12-107 | | |
|---|---|---|---|---|---|---|
| | Holocene | HS1 | LGM | Holocene | HS1 | LGM |
| Core interval | 0.75 cm | 704.25 cm | 848.25 cm | 4.5 cm | 182.5 cm | 272.5 cm |
| | Sample weight (mg CaCO$_3$) / number of individuals | | | Sample weight (mg CaCO$_3$) / number of individuals | | |
| *G. ruber* | 1.10/64 | 1.84/108* | 0.98/57* | 1.61/102 | 7.83/484 | 9.65/500 |
| *T. sacculifer/T.trilobus* | 3.03/91* | 0.71/21 | 1.04/31 | 2.87/92 | 3.00/84 | 2.56/78 |
| *G. inflata* | — | — | 0.83/21 | — | 9.01/274 | 7.88/172 |
| *G. truncatulinoides (d)* | 2.22/65 | 0.61/18 | 1.38/40 | — | 1.27/37 | — |
| *G. crassaformis* | — | 1.18/26 | 0.41/9 | 0.71/22 | — | 0.52/9 |

*Radiocarbon age reported by Lynch-Stieglitz et al. (2014).

Table 2  Overview of planktonic foraminiferal samples from sediment cores KNR166-2-26JPC and VM12-107 and results of $^{14}$C measurement. Radiocarbon ages and errors are reported after Stuiver and Pollach (1977).

| Lab code | Core | Core depth (cm) | Time slice | Species | Method | F$^{14}$C | CO$_2$ final (µgC) | $^{14}$C age (BP) | $^{14}$C age ±1 σ(BP) |
|---|---|---|---|---|---|---|---|---|---|
| BE-8350.1.1 | KNR166-2-26JPC | 0.75 | Holocene | *G. ruber* | Gas | 0.8932 | 123 | 910 | 70 |
| NOSAMS-39884 [Lynch-Stieglitz et al. 2011] | KNR166-2-26JPC | 0.75 | Holocene | *T. sacculifer/T. trilobus* | Graphite | | | 1070 | 70 |
| BE-8351.1.1 | KNR166-2-26JPC | 0.75 | Holocene | *G. truncatulinoides* (d) | Gas | 0.9030 | 162 | 840 | 70 |
| NOSAMS-56991 [Lynch-Stieglitz et al. 2011] | KNR166-2-26JPC | 704.25 | HS1 | *G. ruber* | Graphite | | | 13,500 | 55 |
| BE-9687.1.1 | KNR166-2-26JPC | 704.25 | HS1 | *T. sacculifer/T. trilobus* | Gas | 0.1851 | 41 | 13,560 | 140 |
| BE-8352.1.1 | KNR166-2-26JPC | 704.25 | HS1 | *G. truncatulinoides* (d) | Gas | 0.1642 | 78 | 14,700 | 170 |
| BE-8728.1.1 | KNR166-2-26JPC | 704.25 | HS1 | *G. crassaformis* | Gas | 0.1789 | 119 | 13,870 | 120 |
| NOSAMS-62202 [Lynch-Stieglitz et al. 2011] | KNR166-2-26JPC | 848.25 | LGM | *G. ruber* | Graphite | | | 20,300 | 120 |
| BE-9685.1.1 | KNR166-2-26JPC | 848.25 | LGM | *G. inflata* | Gas | 0.0735 | 112 | 21,030 | 240 |
| BE-9686.1.1 | KNR166-2-26JPC | 848.25 | LGM | *T. sacculifer/T. trilobus* | Gas | 0.0774 | 94 | 20,590 | 240 |
| BE-8353.1.1 | KNR166-2-26JPC | 848.25 | LGM | *G. truncatulinoides* (d) | Gas | 0.0761 | 116 | 20,690 | 300 |
| BE-8729.1.1 | KNR166-2-26JPC | 848.25 | LGM | *G. crassaformis* | Gas | 0.0813 | 41 | 20,370 | 240 |
| BE-8730.1.1 | VM12-107 | 4.5 | Holocene | *G. ruber* | Gas | 0.8821 | 161 | 1020 | 60 |
| BE-9682.1.1 | VM12-107 | 4.5 | Holocene | *T. sacculifer/T. trilobus* | Graphite | 0.8708 | 289 | 1020 | 40 |
| BE-8731.1.1 | VM12-107 | 4.5 | Holocene | *G. crassaformis* | Gas | 0.8549 | 71 | 1250 | 60 |
| BE-8732.1.1 | VM12-107 | 182.5 | HS1 | *G. ruber* | Gas | 0.1763 | 83 | 14,000 | 140 |
| BE-8732.2.1 | VM12-107 | 182.5 | HS1 | *G. ruber* | Graphite | 0.1740 | 675 | 14,070 | 50 |
| BE-8733.1.1 | VM12-107 | 182.5 | HS1 | *G. inflata* | Gas | 0.1640 | 100 | 14,530 | 130 |
| BE-8733.2.1 | VM12-107 | 182.5 | HS1 | *G. inflata* | Graphite | 0.1650 | 825 | 14,500 | 50 |
| BE-9683.1.1 | VM12-107 | 182.5 | HS1 | *T. sacculifer/T. trilobus* | Graphite | 0.1799 | 311 | 13,740 | 60 |
| BE-13191.1.1 | VM12-107 | 182.5 | HS1 | *G. truncatulinoides* (d) | Gas | 0.1641 | 134 | 14,500 | 150 |
| BE-8734.1.1 | VM12-107 | 272.5 | LGM | *G. ruber* | Gas | 0.1012 | 130 | 18,400 | 200 |
| BE-8734.2.1 | VM12-107 | 272.5 | LGM | *G. ruber* | Graphite | 0.1039 | 806 | 18,230 | 60 |
| BE-8735.1.1 | VM12-107 | 272.5 | LGM | *G. inflata* | Gas | 0.1025 | 147 | 18,280 | 190 |
| BE-8735.2.1 | VM12-107 | 272.5 | LGM | *G. inflata* | Graphite | 0.1032 | 696 | 18,290 | 70 |
| BE-9684.1.1 | VM12-107 | 272.5 | LGM | *T. sacculifer/T. trilobus* | Graphite | 0.1041 | 262 | 18,190 | 90 |
| BE-8736.1.1 | VM12-107 | 272.5 | LGM | *G. crassaformis* | Gas | 0.0991 | 52 | 18,640 | 200 |

analyses when compared to solid sample analyses (average: 60 ^{14}C yr; Table 2). All four inter-method replicates produced ^{14}C ages within the analytical uncertainties (average difference: 70 ± 170 ^{14}C yr; supplementary table).

In core KNR166-2-26JPC, the youngest ^{14}C age (840 ± 70 BP) is found not for the mixed-layer species *G. ruber* or *T. sacculifer/T. trilobus,* but for the sub-thermocline calcifying *G. truncatulinoides* (d) (Table 2; Figure 4b). At core site VM12-107, however, *G. crassaformis*, i.e. the deepest calcifying foraminifera, yielded the oldest ^{14}C age (1250 ± 60 BP) and the mixed-layer species *G. ruber* and *T. sacculifer/T. trilobus* give the youngest ^{14}C age (1020 ± 70 BP; Figure 4b), as expected.

For the HS1 time-slice, we observe larger ^{14}C age differences between coexisting planktonic foraminifera than seen for the Holocene (Figure 4d). The mixed-layer planktonic foraminiferal species generally exhibit the youngest ^{14}C ages, with the exception of *G. ruber* in core VM12-107. [14]C ages of the thermocline species *G. inflata* and *G. truncatulinoides* (d) are older than the ^{14}C ages of the mixed-layer species *G. ruber* and *T. sacculifer/T. trilobus* in both cores. At KNR166-2-26JPC, the lower-thermocline calcifying planktonic foraminifer *G. crassaformis* exhibits an age 340 ± 190 BP older than the average age of the surface dwellers. In contrast, *G. truncatulinoides* (d) shows the oldest ^{14}C ages, older by 830 ± 210 BP than *G. crassaformis* (Figure 4d). During the LGM time-slice, ^{14}C ages in core VM12-107 slightly increase from mixed-layer to thermocline-calcifying planktonic foraminifera, similar to the Holocene (Figure 4f). In contrast, ^{14}C ages in core KNR166-2-26JPC are oldest at the upper thermocline similar to HS1 (Figure 4d, f). Apart from our Holocene and LGM ^{14}C ages in core VM12-107, we do not observe a consistent ^{14}C age increase of planktonic foraminifera according to their expected modern calcification depths. Instead, we observe an upper-thermocline maximum of ^{14}C ages during HS1 at both sites and during the LGM at site KNR166-2-26JPC.

The surface to sub-surface ^{14}C age comparison contrasts with the planktonic foraminiferal $\delta^{18}O$ data (Figure 4). The latter shows a consistent increase with the expected calcification depth, with only the upper-thermocline *G. inflata* $\delta^{18}O$ in core VM12-107 during HS1 deviating from this trend. Overall, vertical $\delta^{18}O$ gradients between mixed-layer and thermocline foraminiferal species are less pronounced for the LGM (average over both cores 1.7‰) compared to the Holocene (average over both cores 2.6‰) and weakest for the HS1 time slice, with KNR166-2-26JPC showing a steeper gradient (1.6‰) than VM12-107 (0.7‰). Therefore, while planktonic foraminiferal $\delta^{18}O$ data suggest continuous, albeit variable, upper-ocean stratification at both core sites, our planktonic foraminiferal ^{14}C age gradients do not.

From the multi-species ^{14}C ages we can assess the effect of species choice on dating sediment layers when selecting other species than the shallowest calcifier *G. ruber*, which is most commonly used for dating in tropical and sub-tropical areas. For the inter-species analyses, we observe a maximum difference of 1200 ± 180 ^{14}C yr in core KNR166-2-26JPC during HS1 (*G. ruber* vs. *G. truncatulinoides* (d)). In this case, the choice of species alone could produce significant deviations in ^{14}C ages within one discrete sediment layer clearly exceeding the analytical uncertainties. However, since thermocline calcifiers are commonly avoided for ^{14}C based age models, we compare ^{14}C ages of *G. ruber* to the ages of (i) a hypothetical mix of all available species according to their individual sample weights used in this study, (ii) a hypothetical mixture of *G. ruber* with the other mixed-layer species *T. sacculifer/T. trilobus* to

one single radiocarbon sample, and (iii) the other available mixed layer species (*T. sacculifer/T. trilobus*) alone (Figure 5).

In all but one cases (KNR166-2-26JPC, HS1), blending all available species (mixed-layer and thermocline species) into one $^{14}C$ age according to their individual contributions from their sample weight does not coherently yield a significant bias in $^{14}C$ age from the *G. ruber* sample (Figure 5). While there are clear $^{14}C$ age differences between the species (Figure 4) of one sediment layer, here the relative small sample sizes of the deep calcifiers compared to the more abundant *G. ruber* (Table 1) results in overlapping error bars for both approaches (Figure 5). Similarly, mixing *G. ruber* and. *T. sacculifer/T. trilobus* yields $^{14}C$ ages not significantly different from the pure *G. ruber* result when considering the analytical uncertainty ranges (Figure 5). In two out of six cases significant differences in $^{14}C$ ages can be observed when comparing *G. ruber* and *T. sacculifer/T. trilobus* during HS1 at VM107-12 (with *G. ruber* 330 ± 80 $^{14}C$ yr older, comparing the available graphite $^{14}C$ measurements) and for the Holocene sample at KNR166-2-26JPC (160 ± 100 $^{14}C$ yr younger; Figure 5). Taking into account the analytical uncertainties, the $^{14}C$ age of most subsets of selected species are not statistically different from a pure *G. ruber* sample at our study sites.

## DISCUSSION

### Deviations from the expected increase of planktonic $^{14}C$ ages with calcification depth

For both cores, planktonic foraminiferal $\delta^{18}O$ values increase with modern foraminiferal calcification depth indicating continued upper water column density stratification for the three time slices (Tedesco et al. 2007; Steph et al. 2009). Based on the assumption that deeper water masses within the oceanographic setting of our core locations acquire an older $^{14}C$ signature than the surface ocean, which continuously exchanges with the atmosphere, we expect an increase of $^{14}C$ ages of coexisting planktonic foraminifera with increasing calcification depth in parallel with planktonic foraminiferal $\delta^{18}O$ for all timeslices. If correct, both $\delta^{18}O$ and $^{14}C$ ages from planktonic foraminifera could serve independently as a measure of the upper water column density stratification at our study sites.

Planktonic foraminiferal $^{14}C$ ages in VM12-107 show an expected increase with depth (Figure 4). However, planktonic foraminiferal $^{14}C$ data from KNR166-2-26JPC shows strong deviations from the expected increase in $^{14}C$ ages with depth (Figure 4). For instance, the Holocene *G. truncatulinoides* (d) sample from KNR166-2-26JPC appears too young by at least 350 $^{14}C$ yr to fit onto a linear regression line between $^{14}C$ and $\delta^{18}O$ that would be expected if both parameters are predominantly driven by the density stratification of the water column (Figure 6). Similarly, for HS1, the $^{14}C$ age of *G. crassaformis* deviates from the linear correlation between $^{14}C$ ages and $\delta^{18}O$ dictated by other coexisting planktonic foraminifera (Figure 6b). This might be explained by factors other than a dominant control from the density stratification of the upper water column.

### Factors explaining deviations from expected $^{14}C$ age offsets between planktonic foraminifera

#### Post-Depositional Effects

Offsets in $^{14}C$ ages of coexisting planktonic foraminifera are often related to the post-depositional dissolution of foraminiferal tests. In particular, differential dissolution and fragmentation as a function of size, shape and robustness of shells (Barker et al. 2007;
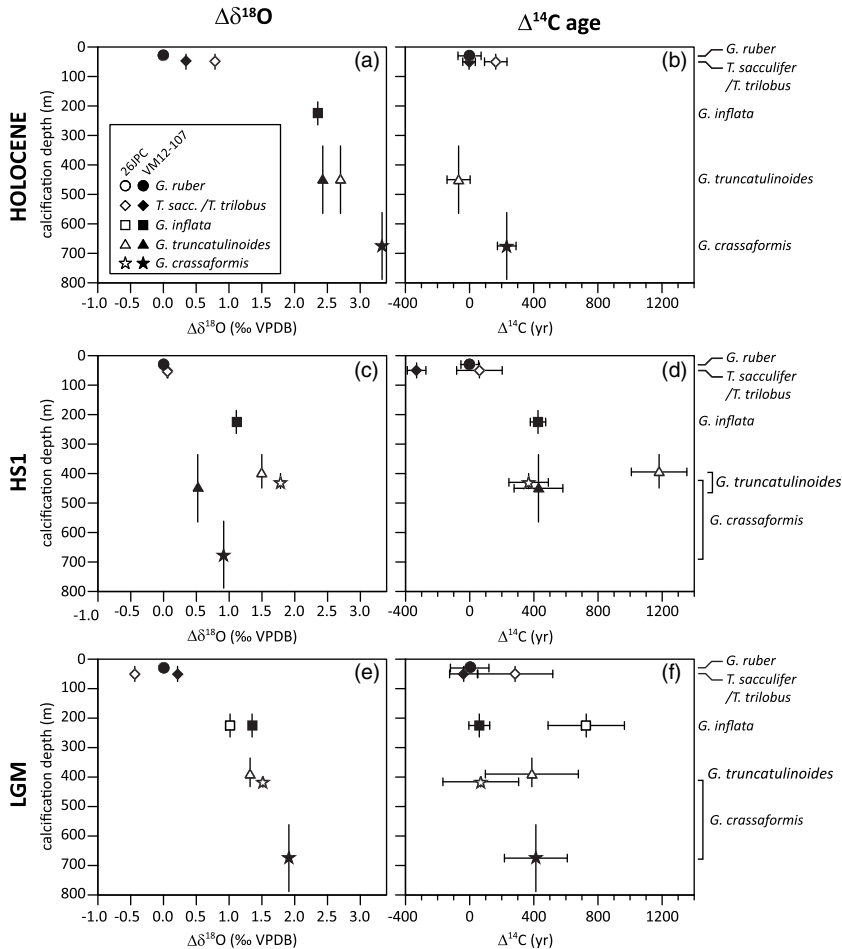
**Figure 4** Planktonic foraminiferal δ¹⁸O (left panels) and ¹⁴C ages (right panels) for the three time slices, Holocene (a, b), HS1 (c, d) and LGM (e, f) from sediment core VM12-107 (black circle) and KNR166-2-26JPC (open square) for five different species (mixed-layer calcifying: *G. ruber*, *T. sacculifer/T. trilobus* and thermocline calcifying: *G. inflata*, *G. truncatulinoides*, *G. crassaformis*, arranged according to their average modern calcification depth as shown in Figure 3). Error bars comprise analytical uncertainties from AMS ¹⁴C measurements (1 sigma) and uncertainties of the habitat- und by inference calcification depth as given in Figure 3. For better comparison between the time-slices and core sites, all data are referenced against *G. ruber*. Due to the shallow water depth of KNR166-2-26JPC (546 m) we assume a more condensed habitat/calcification depth range for *G. crassaformis* and *G. truncatulinoides* shown within an upper range of the intervals depicted in Figure 3. As well lower global sea-levels during HS1 (∼100 m) and the LGM (∼120 m) are considered for KNR166-2-26JPC.

Broecker and Clark 2011) have been identified as a primary effect. However, we consider it very unlikely that dissolution as well as secondary calcification or chemical erosion of foraminiferal tests largely controlled the observed inter-species ¹⁴C ages, given the high sedimentation rates (16–23 and 9–16 cm/kyr) (Schmidt et al. 2012; Lynch-Stieglitz et al. 2014) and the shallow water depths (1079 m and 546 m) of our two study sites, VM12-107 and KNR166-2-26JPC, respectively. Further, the absence of ¹⁴C age reversals throughout the analyzed cores (Schmidt et al. 2012; Lynch-Stieglitz et al. 2014) suggests continuous sedimentation and the absence of disturbed sediment sequences.

Bioturbation, i.e., sediment stirring by benthic organisms, causes sediments from the same depth layer to contain a mixture of relocated younger and older material, which exacerbates data and age uncertainties of samples containing small numbers of individual proxy carriers (Trauth 1998). That is because individual species will be preferentially mixed in from adjacent periods of high abundance into sediment horizons of low abundance, which in turn increases age heterogeneity and hence $^{14}C$ age uncertainties of substrates measured from discrete sediment samples beyond analytical uncertainties. Effects of bioturbation on sample heterogeneity are largest when foraminiferal abundances fluctuate and sedimentation rates are low (Löwemark et al. 2008; Trauth 2013). Given the absence of abundance counts of planktonic foraminiferal species for our study cores, we cannot exclude that bioturbation affected the observed $^{14}C$ and $\delta^{18}O$ gradients at our study sites. Given a commonly assumed bioturbation depth of 3–14 cm (Teal et al. 2008), however, sedimentation rate becomes a crucial parameter determining the age range of a sample, and hence potential intra- and inter-species $^{14}C$ age offsets, when a subset of this sample is analysed (Dolman et al. 2021).

Although having selected high accumulating sediment cores bearing a wide spectrum of different well-preserved planktonic foraminiferal species, some thermocline-calcifying species were clearly less abundant compared to *G. ruber* and/or *T. sacculifer/T. trilobus* (Table 1). With the advance of new $^{14}C$ measurement techniques the amount of foraminiferal tests required for a $^{14}C$ measurement has decreased significantly (Wacker et al. 2013), but potential age heterogeneities due to bioturbation may induce a non-negligible source of uncertainties. For example, some samples of *G. crassaformis* comprised only nine individual tests. Such low numbers increase the likelihood of biases from bioturbated individuals. Dolman et al. (2021) systematically analysed changes in foraminiferal $^{14}C$ age uncertainties as a function of the number of individual tests analysed as well as the bioturbation depth and the sedimentation rate. When assuming a bioturbation of 6 cm, i.e. the global mean (Teal et al. 2008), and applying the approach of Dolman et al. (2021), the $^{14}C$ age uncertainty of our data increases in the worst case by 400% and in the best case by only 3%. In the first case, the relatively low sedimentation rate during the Holocene (~9 cm/kyr) at VM12-107 along with only nine individuals of *G. crassaformis* results in an additional error of 240 $^{14}C$ yr. In contrast, the latter example benefits from ~500 individual *G. ruber* tests and a sedimentation rate of ~16 cm/kyr yielding an additional age error of 17 yr only. In general, the samples containing low amounts of individuals exhibit the highest level of uncertainty as the result of poorer counting statistics (Gottschalk et al. 2018). The error bars of these $^{14}C$ ages could have been reduced only by gathering significantly more tests (e.g., >50) for each species.

*Changes in Foraminiferal Calcification Depths*
The possibility of past shifts of the calcification depth of planktonic foraminifera makes interpretation of past inter-species $^{14}C$ age offsets as indicator of upper-ocean $^{14}C$ gradients difficult. The calcification depth reflects the preference of planktonic foraminiferal species for particular environmental conditions, including seawater $[CO_3^{2-}]$, oxygen concentration, temperature, light availability and nutrient concentration (e.g., (Kucera 2007)). These conditions are intrinsically related to water depth, as well as the planktonic foraminiferal $\delta^{18}O$ reflecting the calcification depth of the species under investigation (Tedesco et al. 2007; Aldridge et al. 2012; Osborne et al. 2016; Rufino et al. 2022;). Some species, however, seem to prefer a constant habitat depth (Rebotim et al. 2019). For instance Groeneveld and Chiessi (2011) found *G. inflata* to occupy a fairly constant depth habitat within the permanent thermocline throughout different hydrographic conditions between 350 and 400 m. Other planktonic foraminifera exhibit specific seasonal production patterns, and thus have different
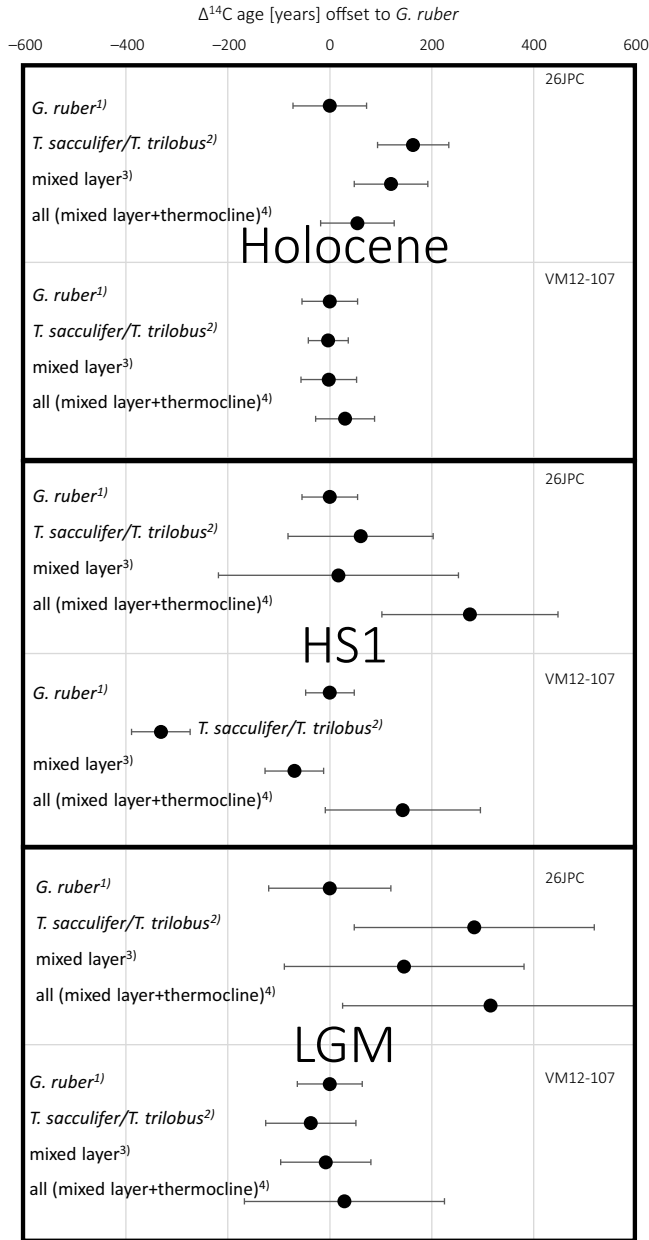
Figure 5   Radiocarbon ages of different subsets of planktonic foraminiferal species relative to *G. ruber* for both sediment cores and three time slices: 1) *G. ruber* $^{14}C$ ages set to 0. 2) $^{14}C$ ages of *T. sacculifer/T. trilobus* relative to *G. ruber*. 3) "mixed layer" indicates the $^{14}C$ ages when *G. ruber* and *T. sacculifer/T. trilobus* would have been mixed, considering the respective sample weights for each species. 4) "all" gives the $^{14}C$ ages when all available species would have been mixed, considering the respective sample weights for each species.
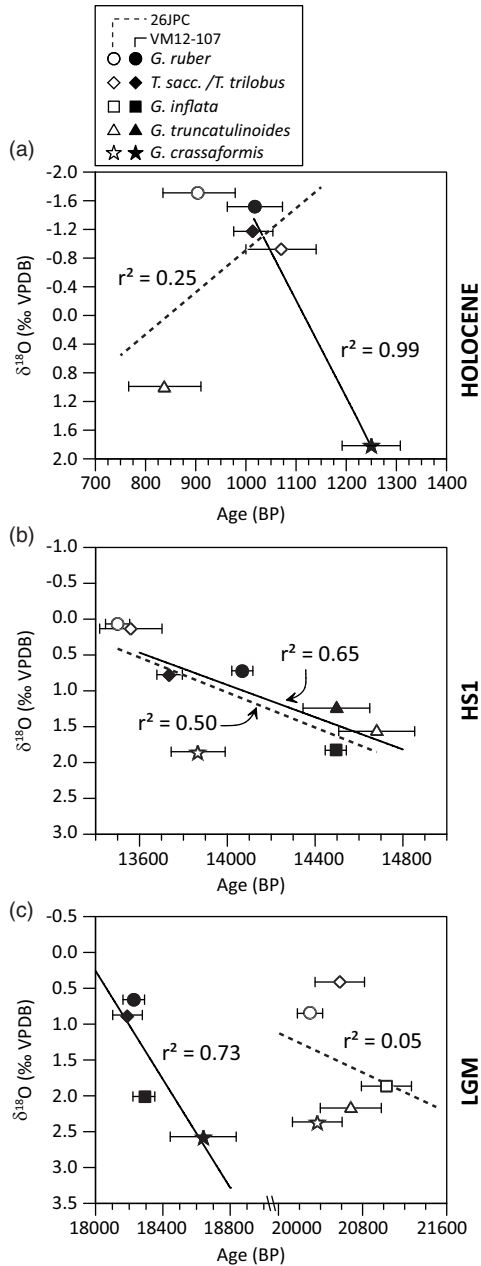
Figure 6   Planktonic foraminiferal $\delta^{18}O$ versus radiocarbon age for the three examined time slices (a: Holocene, b: HS1, c: LGM) from sediment core VM12-107 and KNR166-2-26JPC for available data pairs. In contrast to observations in KNR166-2-26JPC, data from VM12-107 follow a discernible linear relation (though for the Holocene defined by the shallowest and deepest species only) between planktonic foraminiferal $\delta^{18}O$ and $^{14}C$ age.

preferred habitat and calcification depths (Deuser et al. 1981; Tedesco et al. 2007; Jonkers et al. 2015; Lindsay et al. 2015; Salmon et al. 2015; Kretschmer et al. 2018). As a result, calcification depths for individual species may vary over time as a function of the environmental conditions (Jonkers and Kučera 2017). For example, deglacial climate changes have been observed to alter calcification depths of *G. truncatulinoides* in the western tropical Atlantic (Cleroux and Lynch-Stieglitz 2010) and there are observations of *G. crassaformis* habitat depths for instance deviating from the commonly assumed depth ranges (Rebotim et al. 2019). Hence, the calcification depth range for individual species (such as presented in Figure 3) could have deviated from present-day during HS1 and the LGM. In addition, other biological factors, such as different life cycles, potentially add further uncertainty in interpreting the ^{14}C differences among planktonic foraminiferal species. However, our planktonic foraminiferal δ^{18}O data suggests that during HS1 and LGM calcification depths did not deviate strongly from those inferred from present-day observations (Figure 4a,c,e), and hence cannot explain a deviation of planktonic foraminiferal ^{14}C ages from an expected increase with calcification depth as inferred for the present day. In particular, for KNR166-2-26JPC, a hypothetical vertical shift in the calcification depth of multiple planktonic foraminifera, even by a few hundreds of meters, would not be able to explain identical ^{14}C signatures of deep and mixed-layer calcifiers within error and ^{14}C age maxima in the upper thermocline (Figure 4).

## Hydrographic and sedimentary differences between both core sites

Increasing planktonic foraminiferal ^{14}C ages with increasing calcification depths only occur at site VM12-107 (Figure 7). In core KNR166-2-26JPC, a comparison of δ^{18}O with ^{14}C shows that some data points deviate from an approximate linear relation between both isotopic values during the Holocene (*G. truncatulinoides*), HS1 (*G. crassaformis*) and the LGM (*G. crassaformis*). The absence of a correlation between calcification and ^{14}C mostly concerns the deep-dwellers at KNR166-2-26JPC.

### Water depth of KNR166-2-26JPC
Due to the shallow core depth of KNR166-2-26JPC at this location (546 m), the thermocline-calcifying species cannot occupy the full range of their present-day calcification depths (Figure 3) ranging from ~200 to 700 m (*G. truncatulinoides*) and ~500 to 900 m (*G. crassaformis*; Regenberg et al. 2009). This becomes exacerbated during the (de)glaciation, when sea level was lower. Accordingly, during the LGM with a sea-level ~120 m lower than today, calcification depths at KNR166-2-26JPC of these species were at a maximum water depth of ~420 m, limiting the depth of calcification. However, today, the thermocline is compressed and shoaled at this location due to strong currents, allowing Antarctic Intermediate Water that is typically found much deeper offshore to bath our core site. If upper ocean currents substantially weakened during the LGM and HS1, as reconstructions suggest (Lynch-Stieglitz et al. 2014), reduced water depth and thermocline shifts could have forced the lower thermocline calcifiers to become instead upper thermocline-calcifiers. Our planktonic foraminiferal δ^{18}O profiles consistent with the expected depth-profile corroborate that calcification depths did not significantly change during LGM and HS1 (Figure 4a,c,e). Hence, even condensed calcification ranges at site KNR166-2-26JPC during (de)glacial times cannot explain ^{14}C ages of the deepest calcifier *G. crassaformis* to be lower than for assumed calcifiers in the upper water column, i.e., *T. sacculifer/T. trilobus* and *G. inflata*.
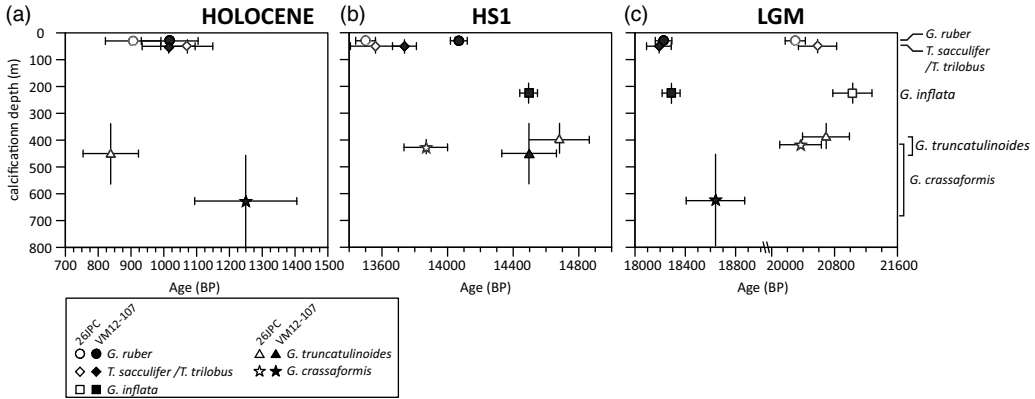
Figure 7  Radiocarbon ages of planktonic foraminifera for the three time slices (a: Holocene, b: HS1, c: LGM) from cores KNR166-2-26JPC and VM12-107 for five different species (in order of average assumed calcification depth) with horizontal error bars comprising analytical uncertainties from AMS measurements and the effects of bioturbation following Dolman et al. (2021). Vertical error bars indicate habitat- and by inference calcification depth ranges as depicted in Figure 3. Due to the shallow water depth of KNR166-2-26JPC (546 m) we assume a more condensed habitat/calcification depth range for *G. crassaformis* and *G. truncatulinoides* shown within an upper range of the intervals depicted in Figure 3. As well lower global sea-levels during HS1 (~100 m) and the LGM (~120 m) are considered for KNR166-2-26JPC.

*Transportation effects at KNR166-2-26JPC*

Deep dwelling species *G. truncatulinoides* and *G. crassaformis*, which are thought to follow an annual life cycle (Deuser et al. 1981; Lohmann and Malmgren 1983; Lohmann 2006; Cléroux et al. 2009), might get transported for long distances (up to several hundred km) by ocean currents before deposition, and thus may not record in-situ conditions at the site of deposition (van Sebille et al. 2015). The potential influence of displaced specimens is less important for the upper thermocline and mixed-layer dwelling species *G. inflata, G. ruber, T. sacculifer,* and *T. trilobus*, which reproduce in a monthly or 15-day cycle with a short life span of a few days (Berger and Soutar 1967; Schiebel et al. 1997; Jonkers and Kučera 2015; Schiebel and Hemleben 2017). Thus, the mismatch between $^{14}C$ ages and $\delta^{18}O$ at KNR166-2-26JPC might be also explained by the deposition of allochthonous tests which would enhance the noise of the proxy signal, in particular because extraordinarily strong bottom currents are active at this site. In the Florida Straits, sedimentary evidence indicates a variable but continuous and strong Florida Current throughout the last ~40,000 yr (Lynch-Stieglitz et al. 2014). Being directly exposed to the main flow of this strong current (Leaman et al. 1995), planktonic foraminifera might get mobilized and subjected to transport to site KNR166-2-26JPC from other locations. Since the horizontal advection distance of foraminiferal tests (living and post-mortem) has been estimated to reach a few hundred kilometres (Siegel and Deuser 1997; v. Gyldenfeldt et al. 2000; van Sebille et al. 2015), this effect is likely at its maximum extent in the highly dynamical environment of the Florida Straits (Hamilton et al. 2005). Depending on the strength of ocean currents at the specific calcification depths of the species, foraminifera may drift from distal areas incorporating isotopic signals along their trajectory into their shells different from the ocean state at the core site. Without high-resolution modeling of the study region for different climate boundary conditions, the effect of advection processes of foraminiferal test on our results cannot be excluded, let alone quantified.

Overall, despite the high abundance of planktonic foraminifera species at site KNR166-2-26JPC, our data demonstrate that unfavourable parameters such as shallow water depth,

bottom currents, and bioturbation in combination or separately can diminish the ability of coexisting planktonic foraminifera to record the upper-ocean $^{14}$C variability. On the other hand, our study site VM12-107 indicates that under more favourable circumstances (less dynamic environment, good preservation, and high sedimentation rate) planktonic foraminiferal $^{14}$C ages are in principle able to track the upper-ocean $^{14}$C age gradients in the past. Even when correcting $^{14}$C age uncertainties for the effects of bioturbation, the $^{14}$C age increase with (present-day) calcification depth is evident at site VM12-107 (Figure 7), which is qualitatively to be expected given the modern hydrography.

### Planktonic foraminiferal $^{14}$C age offsets as indicator of upper ocean stratification at site VM12-107

In addition, at site VM12-107, we observe a general increase of $^{14}$C ages of coexisting planktonic foraminifera with increasing calcification depth in parallel with $\delta^{18}$O for all examined time slices, yet with a different slope for HS1 (Figure 6). It was shown that the equatorial Atlantic thermocline was at a deeper water level during HS1 compared to the Holocene because of surface water cooling during AMOC slowdowns, while subsurface waters warmed (Figure 4; Schmidt et al. 2012; Lynch-Stieglitz et al. 2014). The same processes operated, albeit in weaker fashion, during the LGM (Reißig et al. 2019). In line with these reconstructions, at VM12-107 weak planktonic foraminiferal $\delta^{18}$O gradients suggest a weaker upper ocean stratification during HS1 and the LGM, while steepening occurred towards the Holocene (Figure 4). Accordingly, for HS1 and LGM, we would expect the smallest difference in $^{14}$C ages between mixed-layer versus thermocline-calcifying planktonic foraminifera at site VM12-107, because weaker stratification would facilitate the vertical exchange within the water column, and turbulent mixing would transport atmospheric $^{14}$C more effectively to deeper water layers. However, we observe the largest difference in $^{14}$C ages between mixed-layer versus thermocline-calcifying planktonic foraminifera during HS1 (600 ± 190 $^{14}$C yr) compared to LGM (430 ± 240 $^{14}$C yr) and the Holocene (230 ± 100 $^{14}$C yr). The larger gradients in $^{14}$C ages during HS1 may result from substantially elevated $^{14}$C reservoir ages during this time period (Hodell et al. 2017; Stern and Lisiecki 2013), which would particularly affect the deeper thermocline calcifiers within a weakly stratified water column. Indeed, an increase in reservoir ages over HS1 and the LGM have been inferred for sub-polar, sub-tropical and tropical surface waters along the West Atlantic continental margin (Balmer et al. 2016; Butzin et al. 2017) as a consequence of a reduced AMOC and increased inflow of Antarctic Intermediate Water (Waelbroeck et al. 2001; Stern and Lisiecki 2013; Balmer et al. 2016; Poggemann et al. 2017; Ng et al. 2018; Süfke et al. 2019). It appears that mixing from below of waters carrying a higher reservoir age over-compensates for down-mixing of surface water high in $^{14}$C, facilitated by weaker density stratification. This, eventually, could have led to the larger gradient in $^{14}$C ages between mixed-layer and thermocline calcifiers during HS1 and LGM despite a weaker stratification of the upper water column at site VM12-107.

### CONCLUSIONS

Based on 24 $^{14}$C measurements of coexisting planktonic foraminifera from two sediment cores from the Caribbean Sea and Florida Straits and from three different time slices (Holocene, HS1 and LGM), we examined $^{14}$C ages of coexisting planktonic foraminifera as a function of calcification depth and past changes in water column density stratification. We also assessed the effects of $^{14}$C dating of different planktonic foraminifera species on $^{14}$C-based age models for our study sites. We found that the $^{14}$C age of coexisting planktonic foraminifera differs by

up to 1200 ± 180 $^{14}C$ yr in our study area (i.e., *G. ruber* versus *G. truncatulinoides* at KNR166-2-26JPC during HS1). Radiocarbon dating of thermocline-calcifying planktonic foraminifera or combined $^{14}C$ analyses of thermocline- and mixed layer-species mostly resulted in $^{14}C$ ages older than mixed layer-calcifiers for the same sediment horizon. In our study, however, $^{14}C$ age offsets between mono-specific *G. ruber* $^{14}C$ ages and the $^{14}C$ age of a combined sample (blending all available mixed layer and thermocline calcifying individuals under consideration of their individual weights) reach a maximum of 320 ± 120 $^{14}C$ yr (i.e., at KNR166-2-26JPC during LGM). Any offsets between *G. ruber* and mixed-species $^{14}C$ ages fall within the analytical uncertainties of the $^{14}C$ dates. Hence, if based on mixed planktonic species samples, at our core sites age models would not be significantly biased compared to solely *G. ruber*-based $^{14}C$ dates (maximum of ~6% deviation in $^{14}C$ age, i.e., KNR166-2-26JPC for the Holocene).

Our $^{14}C$ analyses were complemented by planktonic foraminiferal $\delta^{18}O$ measurements that are strongly controlled by the density stratification of the upper water column. During all time intervals under investigation, i.e., the Holocene, HS1 and the LGM, planktonic foraminiferal $\delta^{18}O$ signatures increase with expected modern calcification depths suggesting continuous upper-ocean stratification and broadly consistent calcification depths of the analysed foraminiferal species. In contrast, $^{14}C$ ages do not consistently increase with inferred calcification depth during the analysed time slices. In particular, the deep-dwellers at the shallower core KNR166-2-26JPC within the vigorous Florida Current system showed similar $^{14}C$ ages to coexisting mixed-layer planktonic foraminiferal species with an upper-thermocline maximum in $^{14}C$ ages. This might be driven by stronger mixing in the upper water column in the dynamic environment of the Florida Strait, transport of allochthonous tests from other regions via currents, or the shallow water depth at core site KNR166-2-26JPC that likely puts limitations to deep calcification depths preferred by lower thermocline-calcifying planktonic foraminifera.

In contrast, $^{14}C$ ages from VM12-107 from the Eastern Caribbean Sea increase with inferred calcification depths, even when effects of bioturbation after Dolman et al. (2021) on planktonic foraminiferal $^{14}C$ ages are considered. Thermocline- and mixed-layer calcifying foraminifera thus qualitatively represent the pre-bomb $^{14}C$ profile of the upper water column at this site throughout the analyzed time interval. $^{14}C$ age uncertainties, however, are too large for assessing changes in the magnitude of density stratification of the upper water column. Although a thermocline deepening in the low latitudes of the Atlantic Ocean has been independently reconstructed for HS1 and the LGM, a decrease in the $^{14}C$ age offset between mixed-layer and thermocline calcifying planktonic foraminifera during HS1 cannot be identified. A larger increase in ocean reservoir ages at the thermocline likely resulted in an enhanced $^{14}C$ age offset between mixed-layer and thermocline calcifying foraminifera during periods of weaker AMOC such as HS1 and LGM, masking the effect of decreased upper-ocean density stratification.

Overall, we found that mixed-layer and thermocline-calcifying planktonic foraminifera monitor $\Delta^{14}C$ variations of the upper water column, yet the $^{14}C$ signatures are possibly masked by bioturbation, selective dissolution, sample heterogeneities, variations of the calcification depths of the examined foraminiferal species, and/or analytical $^{14}C$ age uncertainties. In addition, reservoir age changes, (de)glacial variations of the water depth in regions shallower than 900 m (the maximum reported habitat depth of *G. crassaformis*; Figure 3) and hydrographic dynamics in the water column also represent important influencing factors influencing planktonic foraminiferal $^{14}C$ ages. All these factors, which are mostly dependent on the locality, should be taken into account for the interpretation of $^{14}C$ ages of coexisting

planktonic foraminiferal species, especially with regard to their representation of $\Delta^{14}C$ profiles of the upper water column in the past. Our results are relevant for a regional context, whereby lessons learnt are transferable to the wider ocean region.

The main obstacle to decipher robust $^{14}C$ ages from mono-specific planktonic foraminifera is the analytical measurement uncertainty, in particular when considering sample heterogeneities introduced by bioturbation. It is recommended, that future attempts of reconstructing calcification depth related $^{14}C$ age gradients in the past should in the first place focus on increasing the sample sizes, while analysing abundance peaks of the planktonic foraminiferal species under investigation, where possible, and choosing high sedimentation rates sites (>10 cm/kyr) in order to lower the effects of bioturbation. Further, only sediment cores sites that cover the full habitat depth range of deep-calcifying foraminifera (e.g., down to 900 m for *G. crassaformis*) and that are not situated within a vigorous dynamical hydrographic setting should be involved, in order to avoid potential bias that may plague our core site KNR166-2-26JPC.

## SUPPLEMENTARY MATERIAL

For supplementary material accompanying this paper visit https://doi.org/10.1017/RDC.2023.69

## REFERENCES

Aldridge D, Beer CJ, Purdie DA. 2012. Calcification in the planktonic foraminifera *Globigerina bulloides* linked to phosphate concentrations in surface waters of the North Atlantic Ocean. Biogeosciences 9(5):1725–1739.

Andree M, Beer J, Oeschger H, Broecker W, Mix A, Ragano N, O'Hara P, Bonani G, Hofmann HJ, Morenzoni E et al. 1984. $^{14}C$ measurements on foraminifera of deep sea core V28–238 and their preliminary interpretation. Nuclear Instruments and Methods in Physics Research Section B: Beam Interactions with Materials and Atoms 5(2):340–345.

Ascough PL, Cook GT, Dugmore AJ. 2009. North Atlantic marine $^{14}C$ reservoir effects: Implications for late-Holocene chronological studies. Quaternary Geochronology 4(3): 171–180.

Ausin B, Haghipour N, Wacker L, Voelker A, Hodell D, Magill C, Looser N, Bernasconi S, Eglinton T. 2019. Radiocarbon age offsets between two surface dwelling planktonic foraminifera species during abrupt climate events in the SW Iberian Margin. Paleoceanography and Paleoclimatology 34(1):63–78.

Bahr A, Nürnberg D, Karas C, Grützner J. 2013a. Millennial-scale versus long-term dynamics in the surface and subsurface of the western North Atlantic Subtropical Gyre during Marine Isotope Stage 5. Global and Planetary Change 111:77–87.

Bahr A, Nürnberg D, Schönfeld J, Garbe-Schönberg D. 2011. Hydrological variability in Florida straits during Marine isotope stage 5 cold events. Paleoceanography 26(2).

Bahr A, Schönfeld J, Hoffmann J, Voigt S, Aurahs R, Kucera M, Flögel S, Jentzen A, Gerdes A. 2013b. Comparison of Ba/Ca and $\delta^{18}O_{WATER}$ as freshwater proxies: A multi-species core-top study on planktonic foraminifera from the vicinity of the Orinoco River mouth. Earth and Planetary Science Letters 383:45–57.

Balmer S, Sarnthein M, Mudelsee M, Grootes PM. 2016. Refined modeling and $^{14}C$ plateau tuning reveal consistent patterns of glacial and deglacial $^{14}C$ reservoir ages of surface waters in low-latitude Atlantic. Paleoceanography 31(8):1030–1040.

Bard E, Arnold M, Duprat J, Moyes J, Duplessy JC. 1987. Reconstruction of the last deglaciation: Deconvolved records of $\delta^{18}O$ profiles, micropaleontological variations and accelerator

mass spectrometric $^{14}C$ dating. Climate Dynamics 1(2):101–112.

Barker S, Broecker W, Clark E, Hajdas I. 2007. Radiocarbon age offsets of foraminifera resulting from differential dissolution and fragmentation within the sedimentary bioturbated zone. Paleoceanography 22(2).

Berger WH, Soutar A. 1967. Planktonic foraminifera: field experiment on production rate. Science 156(3781):1495–1497.

Boyer TP, Antonov JI, Baranova OK, Coleman C, Garcia HE, Grodsky A, Johnson DR, Locarnini RA, Mishonov AV, O'Brien TD, Paver CR, Reagan JR, Seidov D, Smolyar IV, Zweng MM. 2013. World Ocean Database 2013. NOAA Atlas NESDIS 72. https://dx.doi.org/http://doi.org/10.7289/V5NZ85MT

Broecker W, Barker S, Clark E, Hajdas I, Bonani G. 2006. Anomalous radiocarbon ages for foraminifera shells. Paleoceanography 21(2).

Broecker W, Mix A, Andree M, Oeschger H. 1984. Radiocarbon measurements on coexisting benthic and planktic foraminifera shells: potential for reconstructing ocean ventilation times over the past 20 000 years. Nuclear Instruments and Methods in Physics Research Section B: Beam Interactions with Materials and Atoms 5(2): 331–339.

Broecker W, Clark E. 2011. Radiocarbon-age differences among coexisting planktic foraminifera shells: the Barker Effect. Paleoceanography 26(2). https://doi.org/10.1029/2011PA002116

Butzin M, Köhler P, Lohmann G. 2017. Marine radiocarbon reservoir age simulations for the past 50,000 years. Geophysical Research Letters 44(16):8473–8480.

Chiessi CM, Mulitza S, Paul A, Pätzold J, Groeneveld J, Wefer G. 2008. South Atlantic interocean exchange as the trigger for the Bølling warm event. Geology 36(12):919–922.

Cleroux C, Cortijo E, Duplessy J-C, Zahn R. 2007. Deep-dwelling foraminifera as thermocline temperature recorders. Geochemistry, Geophysics, Geosystems 8(4).

Cleroux C, Lynch-Stieglitz J. 2010. What caused G. truncatulinoides to calcify in shallower water during the early Holocene in the western Atlantic/Gulf of Mexico? IOP Conference Series: Earth and Environmental Science 9:012020.

Cléroux C, Lynch-Stieglitz J, Schmidt MW, Cortijo E, Duplessy J-C. 2009. Evidence for calcification depth change of Globorotalia truncatulinoides between deglaciation and Holocene in the Western Atlantic Ocean. Marine Micropaleontology 73(1):57–61.

Cook MS, Keigwin LD. 2015. Radiocarbon profiles of the NW Pacific from the LGM and deglaciation: Evaluating ventilation metrics and the effect of uncertain surface reservoir ages. Paleoceanography 30(3):174–195.

Deuser WG, Ross EH, Hemleben C, Spindler M. 1981. Seasonal changes in species composition, numbers, mass, size, and isotopic composition of planktonic foraminifera settling into the deep Sargasso Sea. Palaeogeography, Palaeoclimatology, Palaeoecology 33(1):103–127.

Dolman AM, Groeneveld J, Mollenhauer G, Ho SL, Laepple T. 2021. Estimating bioturbation from replicated small-sample radiocarbon ages. Paleoceanography and Paleoclimatology 36: e2020PA004142.

Ezat MM, Rasmussen TL, Thornalley DJR, Olsen J, Skinner LC, Hönisch B, Groeneveld J. 2017. Ventilation history of Nordic Seas overflows during the last (de)glacial period revealed by species-specific benthic foraminiferal $^{14}C$ dates. Paleoceanography 32(2):172–181.

Fairbanks RG, Sverdlove M, Free R, Wiebe PH, Bé AW. 1982. Vertical distribution and isotopic fractionation of living planktonic foraminifera from the Panama Basin. Nature 298(5877): 841–844.

Fairbanks RG, Wiebe PH, Bé AW. 1980. Vertical distribution and isotopic composition of living planktonic foraminifera in the western North Atlantic. Science 207(4426):61–63.

Gottschalk J, Szidat S, Michel E, Mazaud A, Salazar G, Battaglia M, Lippold J, Jaccard S. 2018. Radiocarbon Measurements of Small-Size Foraminiferal Samples with the Mini Carbon Dating System (MICADAS) at the University of Bern: implications for Paleoclimate Reconstructions. Radiocarbon 60(2):1–23.

Groeneveld J, Chiessi C. 2011. Mg/Ca ratios of Globorotalia inflata as a recorder of permanent thermocline temperatures in the South Atlantic. Paleoceanography 26(2):PA2203.

Hamilton P, Larsen JC, Leaman KD, Lee TN, Waddell E. 2005. Transports through the Straits of Florida. Journal of physical oceanography 35(3):308–322.

Hodell DA, Nicholl JA, Bontognali TRR, Danino S, Dorador J, Dowdeswell JA, Einsle J, Kuhlmann H, Martrat B, Mleneck-Vautravers MJ et al. 2017. Anatomy of Heinrich Layer 1 and its role in the last deglaciation. Paleoceanography 32(3): 284–303.

Jentzen A, Nürnberg D, Hathorne EC, Schönfeld J. 2018a. Mg/Ca and $\delta^{18}O$ in living planktic foraminifers from the Caribbean, Gulf of Mexico and Florida Straits. Biogeosciences 15(23): 7077–7095.

Jentzen A, Schönfeld J, Schiebel R. 2018b. Assessment of the effect of increasing temperature on the ecology and assemblage structure of modern planktic foraminifers in the Caribbean and surrounding seas. Journal of Foraminiferal Research 48(3):251–272.

Jonkers L, Kučera M. 2015. Global analysis of seasonality in the shell flux of extant planktonic Foraminifera. Biogeosciences 12(7):2207–2226.

Jonkers L, Kučera M. 2017. Quantifying the effect of seasonal and vertical habitat tracking on planktonic foraminifera proxies. Clim. Past 13(6):573–586.

Jonkers L, Zahn R, Thomas A, Henderson G, Abouchami W, François R, Masque P, Hall IR, Bickert T. 2015. Deep circulation changes in the central South Atlantic during the past 145 kyrs reflected in a combined $^{231}$Pa/$^{230}$Th, neodymium isotope and benthic record. Earth and Planetary Science Letters 419(0):14–21.

Kretschmer K, Jonkers L, Kucera M, Schulz M. 2018. Modeling seasonal and vertical habitats of planktonic foraminifera on a global scale. Biogeosciences 15(14):4405–4429.

Kucera M. 2007. Chapter six planktonic foraminifera as tracers of past oceanic environments. In: Hillaire-Marcel C, De Vernal A, editors. Developments in marine geology. Elsevier. p. 213–262.

Küssner K, Sarnthein M, Lamy F, Tiedemann R. 2018. High-resolution radiocarbon records trace episodes of Zoophycos burrowing. Marine Geology 403:48–56.

Leaman KD, Vertes PS, Atkinson LP, Lee TN, Hamilton P, Waddell E. 1995. Transport, potential vorticity, and current/temperature structure across Northwest Providence and Santaren Channels and the Florida Current off Cay Sal Bank. Journal of Geophysical Research: Oceans 100(C5):8561–8569.

Lindsay CM, Lehman SJ, Marchitto TM, Ortiz JD. 2015. The surface expression of radiocarbon anomalies near Baja California during deglaciation. Earth and Planetary Science Letters 422:67–74.

Lohmann G. 2006. A model for variation in the chemistry of planktonic foraminifera due to secondary calcification and selective dissolution. Paleoceanography, 10: 445–458.

Lohmann GP, Malmgren BA. 1983. Equatorward migration of Globorotalia truncatulinoides ecophenotypes through the Late Pleistocene: gradual evolution or ocean change? Paleobiology 9(4):414–421.

Locarnini RA, Mishonov AV, Baranova OK, Boyer TP, Zweng MM, Garcia HE, Reagan JR, Seidov D, Weathers KW, Paver CR, Smolyar IV. 2019. World Ocean Atlas 2018. Volume 1: temperature. Mishonov A, technical editor. NOAA Atlas NESDIS 81. 52 p.

Lopes dos Santos RA, Prange M, Castañeda IS, Schefuß E, Mulitza S, Schulz M, Niedermeyer EM, Sinninghe Damsté JS, Schouten S. 2010. Glacial–interglacial variability in Atlantic meridional overturning circulation and thermocline adjustments in the tropical North Atlantic. Earth and Planetary Science Letters 300(3):407–414.

Lynch-Stieglitz J, Schmidt MW, Curry WB. 2011. Evidence from the Florida Straits for Younger Dryas ocean circulation changes. Paleoceanography 26(1):PA1205.

Lynch-Stieglitz J, Schmidt MW, Henry GL, Curry WB, Skinner LC, Mulitza S, Zhang R, Chang P. 2014. Muted change in Atlantic overturning circulation over some glacial-aged Heinrich events. Nature Geoscience 7(2):144–150.

Löwemark L, Grootes PM. 2004. Large age differences between planktic foraminifers caused by abundance variations and Zoophycos bioturbation. Paleoceanography 19(2):PA2001.

Löwemark L, Konstantinou K, Steinke S. 2008. Bias in foraminiferal multispecies reconstructions of paleohydrographic conditions caused by foraminiferal abundance variations and bioturbational mixing: a model approach. Marine Geology 256(1–4):101–106.

Löwemark L, Schäfer P. 2003. Ethological implications from a detailed X-ray radiograph and 14C study of the modern deep-sea Zoophycos. Palaeogeography, Palaeoclimatology, Palaeoecology 192(1):101–121.

Manighetti B, McCave N. 1995. Late glacial and Holocene palaeocurrents around Rockall Bank, NE Atlantic Ocean. Paleoceanography 10.

Mekik F. 2014. Radiocarbon dating of planktonic foraminifer shells: a cautionary tale. Paleoceanography 29(1):13–29.

Missiaen L, Wacker L, Lougheed BC, Skinner L, Hajdas I, Nouet J, Pichat S, Waelbroeck C. 2020. Radiocarbon dating of small-sized foraminifer samples: insights into marine sediment mixing. Radiocarbon 62(2):313–333.

Mollenhauer G, Kienast M, Lamy F, Meggers H, Schneider RR, Hayes JM, Eglinton TI. 2005. An evaluation of $^{14}$C age relationships between co-occurring foraminifera, alkenones, and total organic carbon in continental margin sediments. Paleoceanography 20(1):PA1016.

Ng HC, Robinson LF, McManus JF, Mohamed KJ, Jacobel AW, Ivanovic RF, Gregoire LJ, Chen T. 2018. Coherent deglacial changes in western Atlantic Ocean circulation. Nature Communications 9(1):2947.

Nürnberg D, Böschen T, Doering K, Mollier-Vogel E, Raddatz J, Schneider R. 2015. Sea surface and subsurface circulation dynamics off equatorial Peru during the last~ 17 kyr. Paleoceanography 30(7):984–999.

Olsen A, Lange N, Key RM, Tanhua T, Álvarez M, Becker S, Bittig HC, Carter BR, Cotrim da Cunha L, Feely RA et al. 2019. GLODAPv2.2019 – an update of GLODAPv2. Earth Syst. Sci. Data 11(3):1437–1461.

Osborne EB, Thunell RC, Marshall BJ, Holm JA, Tappa EJ, Benitez-Nelson C, Cai W-J, Chen B. 2016. Calcification of the planktonic foraminifera Globigerina bulloides and carbonate ion concentration: results from the Santa Barbara Basin. Paleoceanography 31(8):1083–1102.

Peng T-H, Broecker WS. 1984. The impacts of bioturbation on the age difference between benthic and planktonic foraminifera in deep sea sediments. Nuclear Instruments and Methods in Physics Research Section B: Beam Interactions with Materials and Atoms 5(2):346–352.

Poggemann D–W, Hathorne EC, Nürnberg D, Frank M, Bruhn I, Reißig S, Bahr A. 2017. Rapid deglacial injection of nutrients into the tropical Atlantic via Antarctic Intermediate Water. Earth and Planetary Science Letters 463:118–126.

Rafter PA, Gray WR, Hines SKV, Burke A, Costa KM, Gottschalk J, Hain MP, Rae JWB, Southon JR, Walczak MH et al. 2022. Global reorganization of deep-sea circulation and carbon storage after the last ice age. Science Advances 8(46):eabq5434.

Rebotim A, Voelker AHL, Jonkers L, Waniek JJ, Schulz M, Kucera M. 2019. Calcification depth of deep-dwelling planktonic foraminifera from the eastern North Atlantic constrained by stable oxygen isotope ratios of shells from stratified plankton tows. J. Micropalaeontol. 38(2):113–131.

Regenberg M, Steph S, Nürnberg D, Tiedemann R, Garbe-Schönberg D. 2009. Calibrating Mg/Ca ratios of multiple planktonic foraminiferal species with $\delta^{18}$O-calcification temperatures: Paleothermometry for the upper water column. Earth and Planetary Science Letters 278(3–4):324–336.

Reißig S, Nürnberg D, Bahr A, Poggemann D-W, Hoffmann J. 2019. Southward displacement of the North Atlantic Subtropical Gyre Circulation System during North Atlantic cold spells. Paleoceanography and Paleoclimatology 34(5):866–885.

Reynolds CE, Richey JN, Fehrenbacher JS, Rosenheim BE, Spero HJ. 2018. Environmental controls on the geochemistry of Globorotalia truncatulinoides in the Gulf of Mexico: Implications for paleoceanographic reconstructions. Marine Micropaleontology 142:92–104.

Rufino MM, Salgueiro E, Voelker AAHL, Polito PS, Cermeño PA, Abrantes F. 2022. Ocean kinetic energy and photosynthetic biomass are important drivers of planktonic foraminifera diversity in the Atlantic Ocean. Frontiers in Marine Science 9:887346.

Salmon KH, Anand P, Sexton PF, Conte M. 2015. Upper ocean mixing controls the seasonality of planktonic foraminifer fluxes and associated strength of the carbonate pump in the oligotrophic North Atlantic. Biogeosciences 12(1):223–235.

Schiebel R, Bijma J, Hemleben C. 1997. Population dynamics of the planktic foraminifer Globigerina bulloides from the eastern North Atlantic. Deep Sea Research Part I: Oceanographic Research Papers 44(9):1701–1713.

Schiebel R, Hemleben C. 2017. Planktic foraminifers in the modern ocean. Berlin, Heidelberg: Springer. ISBN 978-3-662-50295-2

Schlitzer R. Ocean data view [Internet].

Schmidt MW, Chang P, Hertzberg JE, Them TR, Ji L, Otto-Bliesner BL. 2012. Impact of abrupt deglacial climate change on tropical Atlantic subsurface temperatures. Proceedings of the National Academy of Sciences 109(36):14348–14352.

Schmidt MW, Lynch-Stieglitz J. 2011. Florida Straits deglacial temperature and salinity change: Implications for tropical hydrologic cycle variability during the Younger Dryas. Paleoceanography 26(4):PA4205.

Schmuker B, Schiebel R. 2002. Planktic foraminifers and hydrography of the eastern and northern Caribbean Sea. Marine Micropaleontology 46(3):387–403.

Siegel DA, Deuser WG. 1997. Trajectories of sinking particles in the Sargasso Sea: modeling of statistical funnels above deep-ocean sediment traps. Deep Sea Research Part I: Oceanographic Research Papers 44(9):1519–1541.

Skinner LC, Bard E. 2022. Radiocarbon as a dating tool and tracer in palaeoceanography. Reviews of Geophysics 60:e2020RG000720.

Steph S, Regenberg M, Tiedemann R, Mulitza S, Nürnberg D. 2009. Stable isotopes of planktonic foraminifera from tropical Atlantic/Caribbean core-tops: implications for reconstructing upper ocean stratification. Marine Micropaleontology 71(1):1–19.

Stern J, Lisiecki L. 2014. Termination 1 timing in radiocarbon-dated regional benthic $\delta^{18}$O stacks. Paleoceanography 29:127–1142.

Stern JV, Lisiecki LE. 2013. North Atlantic circulation and reservoir age changes over the past 41,000 years. Geophysical Research Letters 40(14):3693–3697.

Stuiver M, Polach HA. 1977. Discussion: reporting of $^{14}$C data. Radiocarbon 19(3):355–363.

Süfke F, Pöppelmeier F, Goepfert T, Regelous M, Koutsodendris A, Blaser P, Gutjah M, Lippold J. 2019. Constraints on the northwestern Atlantic deep water circulation from $^{231}$Pa/$^{230}$Th during the last 30,000 years. Paleoceanography and Paleoclimatology 34(12):1945–1958.

Teal LR, Bulling MT, Parker ER, Solan M. 2008. Global patterns of bioturbation intensity and mixed depth of marine soft sediments. Aquatic Biology 2(3):207–218.

Tedesco K, Thunell R, Astor Y, Muller-Karger F. 2007. The oxygen isotope composition of planktonic foraminifera from the Cariaco Basin, Venezuela: Seasonal and interannual variations. Marine Micropaleontology 62(3):180–193.

Thornalley DJR, Barker S, Broecker WS, Elderfield H, McCave IN. 2011. The deglacial evolution of North Atlantic Deep Convection. Science 331(6014):202–205.

Trauth MH. 1998. TURBO: a dynamic-probabilistic simulation to study the effects of bioturbation on paleoceanographic time series. Computers & Geosciences 24(5):433–441.

Trauth MH. 2013. TURBO2: A MATLAB simulation to study the effects of bioturbation on paleoceanographic time series. Computers & Geosciences 61:1–10.

v. Gyldenfeldt A-B, Carstens J, Meincke J. 2000. Estimation of the catchment area of a sediment trap by means of current meters and foraminiferal tests. Deep Sea Research Part II: Topical Studies in Oceanography 47(9):1701–1717.

van Sebille E, Scussolini P, Durgadoo JV, Peeters FJC, Biastoch A, Weijer W, Turney C, Paris CB, Zahn R. 2015. Ocean currents generate large footprints in marine palaeoclimate proxies. Nature Communications 6(1):6521.

Wacker L, J. Lippold, M. Molnár, Schulz H. 2013. Towards single-foraminifera-dating with a gas ion source. Nuclear Instrument Methods B 294:307–310.

Waelbroeck C, Duplessy J-C, Michel E, Labeyrie L, Paillard D, Duprat J. 2001. The timing of the last deglaciation in North Atlantic climate records. Nature 412(6848):724–727.

Wycech J, Kelly DC, Marcott S. 2016. Effects of seafloor diagenesis on planktic foraminiferal radiocarbon ages. Geology 44(7):551–554.